

DetailCLIP: Detail-Oriented CLIP for Fine-Grained Tasks

Amin Karimi Monsefi*
The Ohio State University
Columbus, Ohio
karimimonsefi.1@osu.edu

Kishore Prakash Sailaja*
The Ohio State University
Columbus, Ohio
prakashsailaja.1@osu.edu

Ali Alilooee
The Ohio State University
Columbus, Ohio
alilooeedolatabad.1@osu.edu

Ser-Nam Lim
University of Central Florida
Orlando, Florida
sernam@ucf.edu

Rajiv Ramnath
The Ohio State University
Columbus, Ohio
ramnath.6@osu.edu

Abstract

*In this paper, we introduce **DetailCLIP**: A **Detail-Oriented CLIP** to address the limitations of contrastive learning-based vision-language models, particularly CLIP, in handling detail-oriented and fine-grained tasks like segmentation. While CLIP and its variants excel in the global alignment of image and text representations, they often struggle to capture the fine-grained details necessary for precise segmentation. To overcome these challenges, we propose a novel framework that employs patch-level comparison of self-distillation and pixel-level reconstruction losses, enhanced with an attention-based token removal mechanism. This approach selectively retains semantically relevant tokens, enabling the model to focus on the image’s critical regions aligned with the specific functions of our model, including textual information processing, patch comparison, and image reconstruction, ensuring that the model learns high-level semantics and detailed visual features. Our experiments demonstrate that DetailCLIP surpasses existing CLIP-based and traditional self-supervised learning (SSL) models in segmentation accuracy and exhibits superior generalization across diverse datasets. DetailCLIP represents a significant advancement in vision-language modeling, offering a robust solution for tasks that demand high-level semantic understanding and detailed feature extraction. <https://github.com/KishorePI/DetailCLIP>.*

1. Introduction

The rapid advancements in computer vision have led to the development of robust models that can understand and interpret

visual data with impressive accuracy. Among these, CLIP (Contrastive Language-Image Pretraining) [38] stands out as a pioneering approach that leverages large-scale contrastive learning between images and text to create a shared embedding space. This has proven immensely successful in tasks like classification, where the model can understand and relate visual content to textual descriptions without direct supervision [25,44,51].

However, while CLIP excels in generalization and high-level semantic understanding, its reliance on contrastive losses presents significant challenges when adapting the model for more granular tasks like image segmentation [28,44,48,58]. Fine-grained tasks like segmentation requires a comprehensive understanding of the entire scene and the precise delineation of object boundaries at the pixel level. However, the global representations learned through contrastive learning often fail to capture this level of detail, leading to suboptimal performance when using CLIP for granular tasks [6,21,23,37,43,55].

Furthermore, traditional self-supervised learning (SSL) approaches [5,14,22,34,56,57], which have gained popularity for their ability to learn from unlabeled data, often prove inadequate when applied to fine-grained tasks. These methods, including contrastive learning [7,17,35,41] or clustering-based techniques [32], primarily focus on learning representations that are useful for high-level tasks such as classification or detection. However, they often fail to capture the intricate details and spatial relationships necessary for precise boundary delineation and detailed feature extraction. This limitation is particularly evident in masked image modeling (MIM) approaches such as MAE [16], SimMIM [47], and iBOT [56], which, while effective at learning global features, struggle to preserve fine-grained details. Consequently, these models often require extensive training epochs to achieve moderate performance improvements, yet still fall short in tasks that demand a high degree of granularity. The lack of textual context in these SSL models further exacerbates their limitations, as they miss the additional semantic guidance that text provides, which is crucial for enhancing the model’s ability to focus on detail-oriented tasks. Incorporating text in the pre-training process can significantly improve the model’s performance by align-

*These authors contributed equally to this work.

ing visual features with rich semantic information, leading to better generalization and more accurate granular tasks [2, 49, 52].

We present DetailCLIP, a novel framework designed to overcome the limitations of traditional CLIP-based models and self-supervised learning approaches in tasks involving detail-oriented analysis. DetailCLIP excels in capturing both high-level semantic understanding and fine-grained details, addressing the critical shortcomings of existing models. With its tailored features, DetailCLIP delivers superior performance in scenarios requiring meticulous attention to detail.

DetailCLIP introduces an attention-focus mechanism, token removal, that selectively retains the most relevant parts of an image, closely linked to the corresponding detailed-oriented tasks and textual descriptions. As illustrated in Figure 1, this mechanism highlights the critical areas of the image that are crucial for the task, ensuring that the model focuses on the most pertinent details. By integrating textual context, DetailCLIP enhances the model’s ability to understand and emphasize the critical aspects of an image that are most relevant to the task at hand. This targeted attention not only helps capture subtle nuances and intricate details but also ensures that these elements are accurately represented in the model’s output.

DetailCLIP addresses the issue of inadequate pixel-level accuracy by integrating a pixel-level reconstruction feature that emphasizes the preservation and reconstruction of detailed image features. This approach enables the model to effectively handle the intricate information required for fine-grained visual tasks, making it particularly effective in scenarios where pixel-level precision is critical. While other models, such as MAE [16] and SimMIM [47], also incorporate pixel-level reconstruction to enhance accuracy, they typically rely on random token removal, which can miss essential details. Our approach differs by employing a token removal process based on an attention-focus mechanism, ensuring that only the most relevant features are preserved. This targeted strategy allows DetailCLIP to excel in tasks where precise pixel-level accuracy is vital, distinguishing it from previous methods.

Moreover, to enhance detail preservation and overall model robustness, DetailCLIP incorporates a self-distillation strategy [5]. In this approach, the model simultaneously acts as both a student and a teacher: the student model learns by reconstructing missing details from masked images, while the teacher model operates on the original, unmasked images. This iterative learning process allows the model to progressively refine and recover intricate features, resulting in more comprehensive and effective feature extraction. This not only enhances segmentation accuracy but also ensures that DetailCLIP performs exceptionally well in coarse-grained tasks like classification, where maintaining high-level semantic integrity alongside detailed feature recognition is crucial. Previous works, such as SLIP [33], MaskCLIP [12], and A-CLIP [48], have employed self-distillation techniques that primarily focus on coarse-grained comparisons between student and teacher models. In contrast, our approach extends this framework by incorporating both coarse-grained and fine-grained comparisons, enabling the model to capture and preserve intricate details more effectively. This comprehensive strategy enhances DetailCLIP’s performance across a wide range of tasks, making it particularly well-suited for tasks that demand high levels of precision.

Finally, similar to CLIP-based models [31, 38], DetailCLIP

emphasizes the crucial connection between vision and language, which is essential for tasks that require a deep understanding of visual content and its associated textual concepts.

To summarize, our contributions are fourfold:

- We introduce a novel token removal mechanism driven by attention, which selectively retains tokens with strong semantic connections to the corresponding text descriptions along with detailed-oriented tasks. This targeted focus allows the model to emphasize the most relevant regions of an image, significantly enhancing its capability to capture fine-grained details.
- Our model implements a self-distillation strategy that compares patch-level features using masked images. This approach helps the model to effectively learn low-level semantic features while maintaining a deep understanding of the image content.
- In addition to patch-level comparisons, our model also employs pixel-level reconstruction of masked images. This technique ensures that the model can accurately reconstruct and preserve intricate visual details, leading to superior performance in tasks that require high precision.
- By addressing the limitations of existing CLIP-based and traditional self-supervised learning approaches, our model achieves a robust balance between high-level semantic understanding and precise detail extraction. This makes it particularly effective for zero-shot tasks and fine-tuning in applications that demand meticulous attention to detail.

2. Related Work

2.1. Self Supervised Learning

In recent years, Self-Supervised Learning (SSL) has emerged as a dominant force in visual pre-training, driven by its ability to extract meaningful visual features from large-scale unlabeled image datasets [1, 3, 39]. Various pre-training strategies have fueled the success of SSL, each focusing on different pretext tasks. Among these, contrastive learning [7, 17, 35, 41], Masked Image Modeling (MIM) [2, 16, 32, 36, 47], Masked Frequency Modeling (MFM) [29, 46, 53], and self-supervised Knowledge Distillation (KD) [5, 8, 9, 22, 56] have garnered significant attention.

Contrastive learning, a popular SSL technique, aligns different views of the same image within a shared embedding space while distinguishing them from views of other images [7, 35]. Although this approach is effective for learning global features, it often faces challenges in handling tasks that require detailed precision, such as image segmentation. The reason is that contrastive learning primarily focuses on aligning overall image representations, which can lead to the neglect of fine-grained, pixel-level details.

On the other hand, Masked Image Modeling (MIM) has shown greater promise for tasks requiring detailed feature extraction. MIM involves masking portions of an image and training models to reconstruct or predict the missing parts, encouraging the model to understand the intricate relationships between visible and hidden regions [2, 16, 47, 49].



Figure 1. This image illustrates the mechanism of token removal. The process selectively eliminates less relevant tokens, retaining only those with strong semantic significance. This approach enhances the model’s focus on the most important aspects of the input, ensuring that critical information is preserved while unnecessary details are discarded.

2.2. CLIP-Based Approaches

The integration of self-supervised learning with vision-language pre-training has driven the development of several CLIP-based models, each striving to bridge the gap between visual and textual data [6,20,26,55]. These models build on the original CLIP framework, introducing innovations to enhance the quality of representations and improve alignment between images and text.

For instance, SLIP [33] enhances CLIP by incorporating self-supervised learning with image-to-image contrastive learning, resulting in richer and more robust visual representations. MaskCLIP [12] advances this concept by integrating masked image modeling, which refines visual features by focusing on specific image regions, ensuring they are more closely aligned with the accompanying text. A-CLIP [48] further refines this approach by implementing an attentive token removal strategy, selectively preserving tokens that are semantically relevant to the text, thereby enhancing the precision of the visual-text alignment.

While these methods enhance the original CLIP model by improving representation learning and efficiency, they primarily focus on global alignment between images and text. This emphasis on global features makes them less effective for detail-oriented tasks, where capturing and preserving fine-grained visual details is crucial [19,21,44,58]. In many of these models, token removal is often random or solely based on textual information [12,48]. In contrast, DetailCLIP addresses these limitations by employing an attention-based mechanism that incorporates both textual information and fine-grained tasks, ensuring better performance in detail-sensitive applications.

3. Method

3.1. Preliminary and Background

CLIP is a pioneering vision-language model developed by Radford et al. [38]. Its central concept is to utilize a large-scale contrastive learning method to align visual and textual representations.

This is accomplished by jointly training an image encoder and a text encoder to increase the similarity between matching image-text pairs while reducing it for mismatched pairs. The training objective of CLIP is based on a symmetric cross-entropy loss applied to cosine similarities between the image and text embeddings. The loss function encourages the correct pairs to have higher similarity than incorrect pairs. More precisely, let I_i and T_j be the embeddings of the i -th image and j -th text in the batch, respectively. The cosine similarity between an image and a text is given by:

$$s_{i,j} = \frac{I_i \cdot T_j}{\|I_i\| \|T_j\|}, \quad (1)$$

The logits are scaled by a learnable parameter τ :

$$\text{logits}_{i,j} = \frac{s_{i,j}}{\tau}, \quad (2)$$

Let N be the number of pairs of image-text in a batch. The loss function for the image-to-text matching is defined as:

$$\mathcal{L}_{I2T} = -\frac{1}{N} \sum_{i=1}^N \log \left(\frac{\exp(\text{logits}_{i,i})}{\sum_{j=1}^N \exp(\text{logits}_{i,j})} \right), \quad (3)$$

Similarly, the loss function for the text-to-image matching is:

$$\mathcal{L}_{T2I} = -\frac{1}{N} \sum_{i=1}^N \log \left(\frac{\exp(\text{logits}_{i,i})}{\sum_{j=1}^N \exp(\text{logits}_{j,i})} \right), \quad (4)$$

Finally, the overall loss for CLIP is the average of the two losses:

$$\mathcal{L}_{CLIP} = \frac{1}{2} (\mathcal{L}_{I2T} + \mathcal{L}_{T2I}), \quad (5)$$

3.2. DetailCLIP Framework

As shown in Figure 2, our framework can be outlined through the following steps, which will be discussed in greater detail.

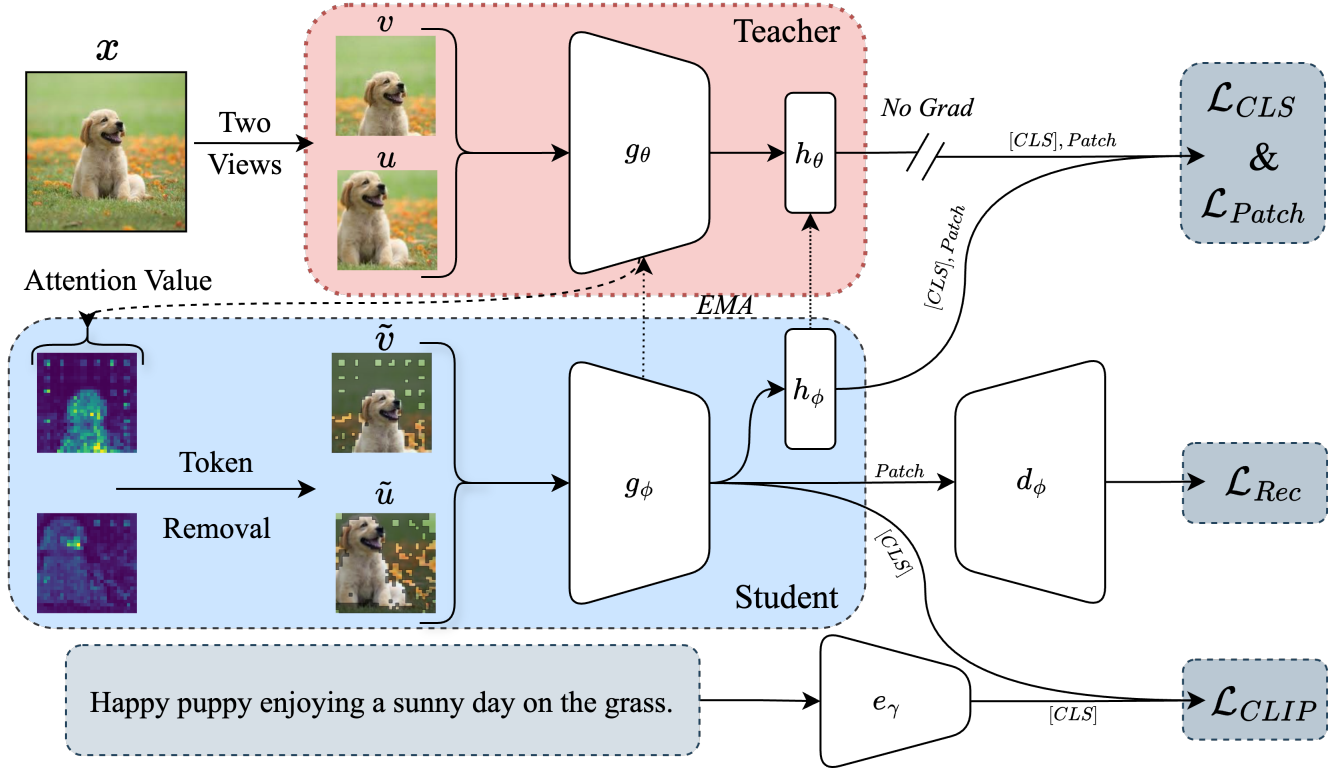


Figure 2. Overview of the DetailCLIP framework for fine-grained segmentation. The framework uses a teacher-student architecture where the teacher model processes two views of the input image x to generate attention values. These values guide the selective token removal process in the student model, focusing on the most semantically relevant parts of the image. The student model then learns to reconstruct the image through a vision decoder while retaining high-level semantic understanding through a combination of classification token loss (\mathcal{L}_{CLS}) patch-level contrastive loss (\mathcal{L}_{Patch}), and pixel-level reconstruction loss (\mathcal{L}_{Rec}). The model also maintains a strong connection between the vision and text encoders using the CLIP loss (\mathcal{L}_{CLIP}), enhancing the model’s segmentation capabilities. In the figure, g is the vision encoder, h is the projection head, d is the image decoder, and e is the text encoder.

3.2.1 Patch-Level Comparison

We employ a teacher-student framework in which the student model is trained to predict both fine-grained and coarse-grained features of images generated by the teacher model. The teacher model provides “target” features for the student to learn. For each input, we consider two views: the original views are fed into the teacher model, while their masked versions are used as input for the student model. For further details on the masking process, refer to Section 3.2.3. The student model is tasked with predicting both the masked tokens and the global features generated by the teacher.

Similar to methods used in previous works like DINO [5], the teacher model’s parameters are updated using an exponential moving average (EMA) of the student model’s parameters and its own. Specifically, if θ represents a parameter of the teacher model and ϕ represents a parameter of the student model, the update rule for θ is $\theta \leftarrow (1 - \lambda)\phi + \lambda\theta$, that λ starting at 0.996 and gradually increasing to 1.0, following a cosine scheduling approach as outlined in previous works [10, 12, 48]. This strategy ensures that the EMA model remains stable and effective in capturing the most relevant

features during training [15].

We employ two primary loss functions to train the student model to ensure both global and fine-grained feature learning are effectively captured.

Global Loss (CLS Token): The global loss, applied to the [CLS] token, measures the difference between the probability distribution of the [CLS] token in the student model and the [CLS] token in the teacher model using KL divergence:

$$\mathcal{L}_{CLS} = D_{KL} \left(p_s^{[CLS]} \parallel p_t^{[CLS]} \right) \quad (6)$$

Where:

- $p_s^{[CLS]}$ is the predicted probability distribution of the [CLS] token from the student model.
- $p_t^{[CLS]}$ is the target probability distribution of the [CLS] token from the teacher model.
- D_{KL} represents the Kullback-Leibler divergence [24].

Fine-grained Loss (Patch): The patch loss also utilizes KL divergence, comparing the distribution of patch tokens in the student

model to those in the teacher model:

$$\mathcal{L}_{\text{patch}} = \frac{1}{|\mathcal{M}|} \sum_{j \in \mathcal{M}} D_{KL} \left(p_s^j \| p_t^j \right) \quad (7)$$

Where:

- \mathcal{M} is the set of indices corresponding to the masked patches.
- p_s^j is the predicted probability distribution of the j -th masked patch from the student model.
- p_t^j is the target probability distribution of the j -th masked patch from the teacher model.
- D_{KL} represents the Kullback-Leibler divergence.

3.2.2 Pixel-Level Reconstruction

As illustrated in Figure 2, following token removal, we employ an autoencoding method (g_ϕ - d_ϕ) (MAE [16]) to reconstruct the original signal from a partially observed input.

By processing only the visible patches, the encoder significantly reduces the amount of data that needs to be handled, thereby improving the model’s efficiency. The decoder is then tasked with reconstructing the original image from the latent representation produced by the encoder. It accomplishes this by using both the encoded visible patches and a set of mask tokens that represent the masked areas. The decoder is smaller and lighter than the encoder, as it is only needed during pre-training. Additionally, by using a smaller decoder, the majority of the computational effort is focused on training the encoder, resulting in a more robust and powerful encoder.

This process is especially well-suited for fine-grained tasks because it pushes the encoder to extract detailed information from the limited visible patches, sharpening its ability to recognize and represent intricate features. By concentrating on these visible patches, the encoder becomes skilled at capturing subtle details that are critical in precision-demanding tasks like segmentation or detailed object recognition. The decoder’s responsibility in reconstructing the masked portions of the image ensures that these fine details are preserved and accurately restored, thereby enhancing the model’s capability to manage complex visual data.

During pre-training, the model learns to reconstruct the original image from the masked input. The loss function (\mathcal{L}_{Rec}) employed during this training is the Mean Squared Error (MSE) between the reconstructed and original images, calculated solely on the masked patches.

$$\mathcal{L}_{\text{Rec}} = \frac{1}{|\mathcal{M}|} \sum_{i \in \mathcal{M}} \|\hat{X}_i - X_i\|^2 \quad (8)$$

where

- \mathcal{M} is the indices corresponding to the masked patches.
- \hat{X}_i is the reconstructed patch for the i -th masked patch.
- X_i is the original patch for the i -th masked patch.
- $\|\cdot\|$ represents the Euclidean norm (or ℓ_2 norm).

3.2.3 Token Removal

Token removal in image models, particularly in ViT, is a strategy to refine the attention mechanism by selectively eliminating tokens that contribute less to the final decision-making process. The token removal method allows the model to dynamically down-weight or ignore less important patches, thereby reducing computational load and focusing attention on the most relevant areas of the image, ultimately enhancing both performance and efficiency.

Various approaches for token removal have been proposed, such as random token removal [22] and attentive token removal [48]. In our work, we introduce a novel technique that considers the specific functions of our model, including textual information processing, patch comparison, and image reconstruction. As demonstrated in 4.2, our token removal strategy outperforms existing methods by addressing both fine-grained and coarse-grained details simultaneously.

As illustrated in Figure 2, our token removal process operates as follows. We first input an image view into the teacher encoder model (g_θ). The attention values generated by the teacher encoder are then used to mask the 50% of patches with the lowest values. Specifically, for each patch p_t the attention values are calculated using the following formula:

$$AV_{p_t} = \frac{1}{N} \sum_{i=1}^N \text{Softmax} \left(\frac{Q_i \cdot K_i(p_t)}{\sqrt{d}} \right) \quad (9)$$

- N is the total number of attention heads across all layers.
- Q_i is the query of the [CLS] from the i -th attention head.
- $K_i(p_t)$ is the key of the patch at position p_t from the i -th attention head.
- d is the dimensionality of the query and key.

As shown in Figure 1, masking image patches by removing the lowest half of the attention values (AV) calculated by the teacher encoder results in the images displayed in the figure.

3.2.4 Integrated Loss Function

In this section, we introduce the formulation of a comprehensive loss function that combines the various loss components essential for effective multi-task learning. The integrated loss function is defined as:

$$\mathcal{L}_{\text{tot}} = \alpha_1 \times \mathcal{L}_{\text{CLS}} + \alpha_2 \times \mathcal{L}_{\text{Patch}} + \alpha_3 \times \mathcal{L}_{\text{Rec}} + \mathcal{L}_{\text{CLIP}}, \quad (10)$$

In this equation, the hyperparameters α_1 , α_2 , and α_3 determine the relative importance of each loss term. These weights are set to 1 in our experiments unless specified otherwise. The comprehensive loss function is designed to enable the model to concurrently learn across the four tasks introduced in previous sections, ensuring a balanced and integrated training process.

Additionally, in the ablation study, we explore the impact of different hyperparameter choices, demonstrating how varying these weights can influence the overall model performance and task-specific outcomes.

Methods	Dataset	Epoch	Effective View	ADE20K		COCO	
				UperNet	Linear	AP ^b	AP ^m
<i>Self-Supervised</i>							
DeiT [42]	IN-1K	300	720M	47.4	-	44.1	39.8
MAE [16]	IN-1K	800	960M	46.5	34.3	46.2	39.1
DINO [5]	IN-1K	800	9600M	46.8	34.5	47.4	40.1
iBOT [56]	IN-1K	300	720M	47.3	34.7	48.4	42.1
AttMask [22]	IN-1K	300	4320M	47.5	35.2	48.9	42.2
<i>CLIP-Based Model</i>							
CLIP [38]	400M	-	-	46.4	34.2	43.6	39.5
SLIP [33]	YFCC-15M	25	750M	46.6	36.1	44.0	40.3
MaskCLIP [12]	YFCC-15M	25	750M	47.5	36.3	45.4	40.9
A-CLIP [48]	YFCC-15M	25	750M	47.0	34.7	45.8	41.7
DetailCLIP	YFCC-15M	25	750M	48.1	37.3	48.9	42.5
DetailCLIP	YFCC-15M	50	1500M	48.8	39.3	50.1	43.3

Table 1. Performance comparison of various models on detail-oriented visual tasks, including segmentation and object detection. All models utilize the vision component’s ViT-B (Vision Transformer Base) architecture. Segmentation results are presented for the ADE20K dataset using UperNet and linear decoders. At the same time, object detection performance is evaluated on the MS COCO dataset with Average Precision for the bounding box. DetailCLIP consistently outperforms other models, particularly in tasks requiring high levels of detail and precision. (“Effective View” is the total number of image views used during training, calculated as the number of views per image multiplied by the number of epochs and size of the dataset. This metric is critical to our evaluation as it reflects the model’s exposure to diverse perspectives of the training data, which directly impacts its ability to generalize and perform well on detail-oriented tasks.)

4. Experiments

4.1. Setup

Our computational setup is designed to support the extensive experiments conducted in this study. It consists of four nodes, each equipped with four NVIDIA A100 GPUs, each with 80GB.

4.1.1 Training Data and Augmentation Strategy

Our model is trained on a carefully curated 15 million image subset [38] of the YFCC100M dataset [40], which contains only English-language titles and descriptions. For each image, a valid caption—either a title or description—is randomly selected during training, following the methodology used in SLIP [33].

To enhance model robustness, we employ a data augmentation strategy similar to that of SLIP. Images are randomly resized and cropped to a size between 50% and 100% of their original dimensions. This augmentation is applied to the images in the online training branches, allowing the model to learn from varied perspectives of the same image.

For the teacher part, a slightly different approach is taken. We use a larger randomly cropped sub-image compared to the online views, which allows us to accurately compute attention value.

4.1.2 Architecture and Training Setting

Figure 2 illustrates the architecture of the DetailCLIP framework, which is composed of six key components: two visual encoders, denoted as g_θ , and g_ϕ , a text encoder named e_γ , a vision decoder named d_ϕ , and two heads referred to as h_θ and h_ϕ .

To ensure a fair comparison with existing models, our visual encoders (g_θ and g_ϕ) are based on the widely recognized Vision

Methods	E	Flickr30K		COCO		IN-1K
		I2T	T2I	I2T	T2I	0-Shot
CLIP	25	51.4	32.6	27.9	17.6	37.6
SLIP	25	57.2	41.2	33.6	21.9	42.8
MaskCLIP	25	60.0	38.8	34.1	21.2	42.7
A-CLIP	25	62.7	42.1	38.0	23.2	43.9
DetailCLIP	25	62.8	42.2	38.3	22.9	43.9
CLIP	50	53.9	35.8	30.2	19.2	39.4
SLIP	50	60.6	41.1	33.2	22.3	44.1
A-CLIP	50	66.7	43.2	39.8	24.4	46.3
DetailCLIP	50	65.9	44.7	39.8	24.9	46.2

Table 2. Performance comparison of various models on text-image retrieval tasks across the Flickr30K and MS COCO datasets, as well as zero-shot evaluation on ImageNet-1K (IN-1K). The table reports results after 25 and 50 epochs (E), showing performance metrics for image-to-text (I2T) and text-to-image (T2I) retrieval on each dataset. The results were collected in the A-CLIP paper [48].

Transformer (ViT-B/16) [13] architecture. This model features 12 layers, each with a width of 768 and 12 attention heads.

For the text encoder (e_γ), we adopted a 12-layer Transformer architecture with a width of 512 and 8 attention heads, following the design principles established by the CLIP model [38].

The decoder (d_ϕ) itself is composed of a series of transformer blocks like MAE paper [16]. The decoder handles the entire set of input patches, including both the attention-masked and retained patches. Positional embeddings are added to each token in the set to preserve the spatial information.

The projection heads (h_θ and h_ϕ) in our framework are implemented as 3-layer MLPs, featuring an L2-normalized bottleneck, similar to the approach used in DINO [5]. The output dimension of the shared projection head is set to 8192 like iBOT paper [56], for robust feature representation and alignment during training.

For our experiments, we employ the *AdamW* optimizer [30] with a learning rate of $5e-4$ and a weight decay of 0.5. The training is conducted with a substantial batch size of 4096.

4.2. Experimental Analysis

4.2.1 Detail-Oriented Visual Tasks

In order to comprehensively evaluate the effectiveness of our proposed DetailCLIP framework, we designed a series of experiments focused on detail-oriented visual tasks. Specifically, we implemented different distinct tasks that emphasize the model’s ability to capture fine-grained details in complex visual environments.

Semantic Segmentation on ADE20K: To evaluate the segmentation capabilities of DetailCLIP, we conducted a series of experiments on the ADE20K dataset [54] using different decoding strategies. First, we tested the model with the UperNet [45] decoder, a well-established architecture for semantic segmentation, to assess its ability to delineate object boundaries and achieve high segmentation accuracy. Next, we employed a linear decoder for segmentation tasks to explore the model’s versatility. This more straightforward approach allowed us to evaluate how well DetailCLIP maintains performance with minimal architectural complexity. These experiments collectively provide a comprehensive understanding of DetailCLIP’s strengths in detail-oriented segmentation tasks.

We utilized the UperNet or linear decoder with an input resolution of 512×512 pixels, conducting end-to-end training for 160k iterations. The performance of our model was evaluated using the mean Intersection over Union (mIoU) metric.

Object Detection and Instance Segmentation on the COCO: This task requires simultaneous object localization and classification, making them complex tasks that demand high precision. For our evaluation, we employed the Cascade Mask R-CNN model [4, 18] like iBOT [56], known for effectively producing bounding boxes and instance masks on the COCO dataset [27]. The evaluation metrics used in this study were the Average Precision for bounding boxes (AP^b) and masks (AP^m).

Evaluating Task Outcomes: Table 1 highlights the significant advantages of DetailCLIP over existing models in various detail-oriented visual tasks. Utilizing the ViT-B architecture, DetailCLIP outperformed other models across multiple benchmarks. For instance, on the ADE20K dataset with the UperNet decoder, DetailCLIP achieved a *mIoU* of 48.8, 1.3 points higher than the closest competitor, MaskCLIP, which recorded a *mIoU* of 47.5. Similarly, in the linear decoder setting, DetailCLIP’s *mIoU* of 39.3 surpasses SLIP’s performance by 3.2 points, highlighting our model’s superior capacity to maintain high performance.

Furthermore, in object detection tasks on the MS COCO dataset, DetailCLIP for bounding boxes achieved 48.9 AP^b , outperforming previous models by as much as 3.1 points, with ACLIP being the closest at 45.8. The mask precision is 42.5 AP^m , further underscoring our model’s effectiveness, exceeding the best-performing alternative by 0.8 points. These substantial improvements demonstrate DetailCLIP’s effectiveness in enhancing high-

level semantic understanding and fine-grained detail extraction, setting a new benchmark in the field.

Visual Comparative Analysis: Figure 5 shows the result of our model compared to the other baselines. We invite you to refer to the appendix. This comparison covers segmentation and object detection tasks, demonstrating DetailCLIP’s enhanced performance.

4.2.2 Image Classification

Zero-shot on Text-Image Retrieval: We also present the zero-shot text-image retrieval on 3 benchmark datasets: Flickr30K [50], MS-COCO [27], and ImageNet-1K [11]. Our findings indicate that using plain text, without any added prefixes or suffixes, consistently yields strong performance across all models evaluated.

Table 2 comprehensively evaluates different models on text-image retrieval tasks, explicitly focusing on Flickr30K and MS-COCO datasets, also a zero-shot evaluation on ImageNet-1K.

At 25 epochs, DetailCLIP demonstrates the highest performance across most metrics, achieving the best results in Flickr I2T (62.8), T2I (42.2), COCO I2T (38.3), and zero-shot on IN-1K (43.9), closely matching A-CLIP. For 50 epochs, DetailCLIP maintains its superior performance, particularly in the COCO dataset, where it ties in with A-CLIP for the best I2T score (39.8) and surpasses A-CLIP in T2I with a score of 24.9. The results suggest that DetailCLIP is particularly strong in tasks that require detailed matching between text and images. DetailCLIP outperforms other models in both datasets’ I2T and T2I retrieval tasks, indicating its effectiveness in text-image association.

Zero-Shot Classification Performance Evaluation on Diverse Benchmarks: We evaluated the zero-shot classification performance of our proposed DetailCLIP approach across 13 different classification tasks, following the evaluation protocols established by SLIP [33]. This included using identical prompts during testing to ensure a fair comparison. This rigorous evaluation framework allowed us to directly assess and compare DetailCLIP’s performance against other leading models.

The results in the table 3 demonstrate that DetailCLIP consistently outperforms its competitors. Specifically, DetailCLIP achieved the highest performance in 12 out of 26 evaluation scenarios and secured the second-best position in 5 additional cases. Notably, DetailCLIP also achieved the highest average scores in both the 25-epoch (37.3) and 50-epoch (37.6) settings, underscoring its robustness and generalization capabilities across a diverse array of benchmarks.

These results highlight DetailCLIP’s effectiveness in zero-shot classification tasks, particularly compared to other state-of-the-art models across various datasets.

4.2.3 Ablation Study on Loss Weight Optimization

In this ablation study, we investigate the impact of different weight configurations on the comprehensive loss function \mathcal{L}_{tot} introduced in Eq. 10. We aim to identify the optimal values for the hyperparameters α_1 , α_2 , and α_3 that effectively balance the various losses.

Table 4 presents the results of this exploration, showing how different combinations of these weights influence the zero-shot accuracy on the ImageNet-1k dataset after 25 epochs of training. The

Epochs	Methods	SUN397	Aircraft	DTD	Pets	Flowers	GTSRB	MNIST	STL-10	KITTI	Country211	PCAM	CLEVR	SST2	Average
25	CLIP	51.1	5.4	21.2	28.5	53.3	6.1	8.4	90.5	35.1	10.5	53.5	10.8	50.7	32.7
	SLIP	53.4	5.7	26.1	31.1	56.6	14.5	9.8	94.4	34.0	11.6	55.4	17.5	51.1	35.5
	MaskCLIP	54.0	8.2	25.5	36.8	53.6	10.1	11.2	93.9	30.5	12.5	51.2	12.9	50.0	34.6
	A-CLIP	57.0	7.6	26.0	32.0	57.7	13.1	9.8	95.4	35.2	13.5	51.6	14.1	49.9	35.6
	DetailCLIP	54.9	8.7	30.1	35.4	60.7	9.3	11.4	94.1	42.2	11.9	62.0	13.4	50.2	37.3
50	CLIP	49.0	6.3	23.5	27.2	56.2	7.4	12.5	92.1	33.6	10.9	50.8	14.0	50.1	33.4
	SLIP	54.8	9.0	29.8	31.9	57.7	9.0	9.8	95.6	35.1	12.7	54.4	13.8	49.9	35.7
	A-CLIP	58.7	10.2	27.7	40.5	61.0	9.4	11.3	95.5	23.3	14.4	63.7	19.6	52.3	37.5
	DetailCLIP	57.5	11.0	29.8	40.8	64.1	7.3	10.8	95.8	30.9	13.3	63.9	12.7	50.1	37.6

Table 3. Zero-shot performance evaluation across multiple classification benchmarks. Epochs indicate the total number of training epochs. The results were collected in the A-CLIP paper [48].

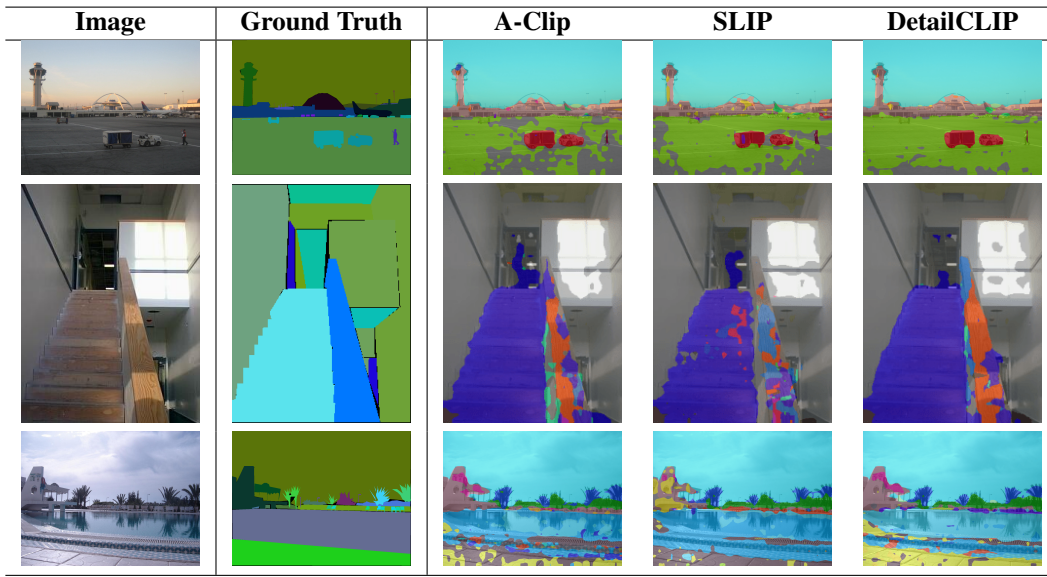


Figure 3. Visual comparison of segmentation results using the Linear decoder across different models. The comparison includes SLIP, Attentive Mask CLIP, and DetailCLIP at 25 epochs.

	$\alpha_1 = 1$	$\alpha_1 = 1$	$\alpha_1 = 1$	$\alpha_1 = .5$	$\alpha_1 = 0$
	$\alpha_2 = 1$	$\alpha_2 = 1$	$\alpha_2 = 1$	$\alpha_2 = .5$	$\alpha_2 = 0$
	$\alpha_3 = 1$	$\alpha_3 = 0$	$\alpha_3 = 2$	$\alpha_3 = .5$	$\alpha_3 = 1$
Acc	43.9	42.9	43.2	43.3	42.6

Table 4. Impact of varying α values on the zero-shot accuracy of ImageNet-1k after 25 epochs of training with the DetailCLIP.

accuracy values reflect the model’s performance under varying degrees of emphasis on each loss term.

Analyzing the results, we find that the baseline configuration, where all weights are set to 1, achieves the highest accuracy of 43.9%, suggesting that equal emphasis on all loss components

provides a robust performance baseline. When α_3 is reduced to 0, thereby ignoring the reconstruction loss, the accuracy slightly decreases to 42.9%, indicating that while this loss component is not critical, it still positively influences overall model performance. Doubling α_3 to 2 results in a marginal accuracy decrease to 43.2%, implying that an overemphasis on the reconstruction loss can detract slightly from the model’s effectiveness in other tasks. Lowering the weights of α_1 and α_2 to 0.5 yields an accuracy of 43.3%, demonstrating that moderate weight reductions do not significantly impact performance. However, eliminating these ($\alpha_1 = 0$ and $\alpha_2 = 0$) reduces accuracy further to 42.6%, underscoring their essential role in the model’s learning process.

5. Conclusion

In this paper, we introduced DetailCLIP, a novel framework designed to overcome traditional CLIP-based models' limitations in fine-grained and coarse-grained tasks. While existing models like CLIP excel at globally aligning image and text representations, they often fail to capture the fine-grained details necessary for tasks such as image segmentation and object detection. To address this, we integrated innovative techniques into DetailCLIP, including patch-level comparison, pixel-level reconstruction, and an attention-based token removal mechanism. These features enable the model to focus on the most critical regions of an image, significantly enhancing its performance in detail-oriented tasks. Our extensive experiments demonstrated that DetailCLIP consistently outperforms state-of-the-art models in tasks requiring high levels of detail, such as segmentation on the ADE20K dataset and object detection on the MS COCO dataset, where it sets new benchmarks in critical metrics like mIoU and Average Precision. Furthermore, DetailCLIP's strength extends beyond fine-grained tasks, as it excels in coarse-grained tasks like zero-shot classification.

References

- [1] Amani Almalki and Longin Jan Latecki. Self-supervised learning with masked autoencoders for teeth segmentation from intra-oral 3d scans. In *Proceedings of the IEEE/CVF Winter Conference on Applications of Computer Vision*, pages 7820–7830, 2024. 2
- [2] Hangbo Bao, Li Dong, Songhao Piao, and Furu Wei. Beit: Bert pre-training of image transformers. In *International Conference on Learning Representations*, 2022. 2
- [3] Ido Ben-Shaul, Ravid Shwartz-Ziv, Tomer Galanti, Shai Dekel, and Yann LeCun. Reverse engineering self-supervised learning. *Advances in Neural Information Processing Systems*, 36, 2024. 2
- [4] Zhaowei Cai and Nuno Vasconcelos. Cascade r-cnn: High quality object detection and instance segmentation. *IEEE transactions on pattern analysis and machine intelligence*, 43(5):1483–1498, 2019. 7
- [5] Mathilde Caron, Hugo Touvron, Ishan Misra, Hervé Jégou, Julien Mairal, Piotr Bojanowski, and Armand Joulin. Emerging properties in self-supervised vision transformers. In *Proceedings of the IEEE/CVF international conference on computer vision*, pages 9650–9660, 2021. 1, 2, 4, 6, 7
- [6] Junbum Cha, Jonghwan Mun, and Byungseok Roh. Learning to generate text-grounded mask for open-world semantic segmentation from only image-text pairs. In *Proceedings of the IEEE/CVF Conference on Computer Vision and Pattern Recognition*, pages 11165–11174, 2023. 1, 3
- [7] Ting Chen, Simon Kornblith, Mohammad Norouzi, and Geoffrey Hinton. A simple framework for contrastive learning of visual representations. In *International conference on machine learning*, pages 1597–1607. PMLR, 2020. 1, 2
- [8] Ting Chen, Simon Kornblith, Kevin Swersky, Mohammad Norouzi, and Geoffrey E Hinton. Big self-supervised models are strong semi-supervised learners. *Advances in neural information processing systems*, 33:22243–22255, 2020. 2
- [9] Xinlei Chen and Kaiming He. Exploring simple siamese representation learning. In *Proceedings of the IEEE/CVF conference on computer vision and pattern recognition*, pages 15750–15758, 2021. 2
- [10] Xinlei Chen, Saining Xie, and Kaiming He. An empirical study of training self-supervised vision transformers. In *Proceedings of the IEEE/CVF international conference on computer vision*, pages 9640–9649, 2021. 4
- [11] Jia Deng, Wei Dong, Richard Socher, Li-Jia Li, Kai Li, and Li Fei-Fei. Imagenet: A large-scale hierarchical image database. In *2009 IEEE conference on computer vision and pattern recognition*, pages 248–255. Ieee, 2009. 7
- [12] Xiaoyi Dong, Jianmin Bao, Yinglin Zheng, Ting Zhang, Dongdong Chen, Hao Yang, Ming Zeng, Weiming Zhang, Lu Yuan, Dong Chen, et al. Maskclip: Masked self-distillation advances contrastive language-image pretraining. In *Proceedings of the IEEE/CVF Conference on Computer Vision and Pattern Recognition*, pages 10995–11005, 2023. 2, 3, 4, 6
- [13] Alexey DOSOVITSKIY. An image is worth 16x16 words: Transformers for image recognition at scale. *arXiv preprint arXiv:2010.11929*, 2020. 6
- [14] Bahar Farahani and Amin Karimi Monsefi. Smart and collaborative industrial iot: A federated learning and data space approach. *Digital Communications and Networks*, 9(2):436–447, 2023. 1
- [15] Jean-Bastien Grill, Florian Strub, Florent Altché, Corentin Tallec, Pierre Richemond, Elena Buchatskaya, Carl Doersch, Bernardo Avila Pires, Zhaohan Guo, Mohammad Gheshlaghi Azar, et al. Bootstrap your own latent—a new approach to self-supervised learning. *Advances in neural information processing systems*, 33:21271–21284, 2020. 4
- [16] Kaiming He, Xinlei Chen, Saining Xie, Yanghao Li, Piotr Dollár, and Ross Girshick. Masked autoencoders are scalable vision learners. In *Proceedings of the IEEE/CVF conference on computer vision and pattern recognition*, pages 16000–16009, 2022. 1, 2, 5, 6
- [17] Kaiming He, Haoqi Fan, Yuxin Wu, Saining Xie, and Ross Girshick. Momentum contrast for unsupervised visual representation learning. In *Proceedings of the IEEE/CVF conference on computer vision and pattern recognition*, pages 9729–9738, 2020. 1, 2
- [18] Kaiming He, Georgia Gkioxari, Piotr Dollár, and Ross Girshick. Mask r-cnn. In *Proceedings of the IEEE international conference on computer vision*, pages 2961–2969, 2017. 7
- [19] Wenbin He, Suphanut Jamonnak, Liang Gou, and Liu Ren. Clip-s4: Language-guided self-supervised semantic segmentation. In *Proceedings of the IEEE/CVF Conference on Computer Vision and Pattern Recognition*, pages 11207–11216, 2023. 3
- [20] Chao Jia, Yinfei Yang, Ye Xia, Yi-Ting Chen, Zarana Parekh, Hieu Pham, Quoc Le, Yun-Hsuan Sung, Zhen Li, and Tom Duerig. Scaling up visual and vision-language representation learning with noisy text supervision. In *International conference on machine learning*, pages 4904–4916. PMLR, 2021. 3
- [21] Siyu Jiao, Yunchao Wei, Yaowei Wang, Yao Zhao, and Humphrey Shi. Learning mask-aware clip representations

- for zero-shot segmentation. *Advances in Neural Information Processing Systems*, 36:35631–35653, 2023. 1, 3
- [22] Ioannis Kakogeorgiou, Spyros Gidaris, Bill Psomas, Yannis Avrithis, Andrei Bursuc, Konstantinos Karantzas, and Nikos Komodakis. What to hide from your students: Attention-guided masked image modeling. In *European Conference on Computer Vision*, pages 300–318. Springer, 2022. 1, 2, 5, 6
- [23] Amin Karimi Monsefi, Pouya Shiri, Ahmad Mohammadshirazi, Nastaran Karimi Monsefi, Ron Davies, Sobhan Moosavi, and Rajiv Ramnath. Crashformer: A multimodal architecture to predict the risk of crash. In *Proceedings of the 1st ACM SIGSPATIAL International Workshop on Advances in Urban-AI*, pages 42–51, 2023. 1
- [24] Solomon Kullback and Richard A Leible. On information and sufficiency. *The Annals of Mathematical Statistics*, 22(1):79–86, 1951. 4
- [25] Mengcheng Lan, Chaofeng Chen, Yiping Ke, Xinjiang Wang, Litong Feng, and Wayne Zhang. Proxyclip: Proxy attention improves clip for open-vocabulary segmentation. *arXiv preprint arXiv:2408.04883*, 2024. 1
- [26] Yanghao Li, Haoqi Fan, Ronghang Hu, Christoph Feichtenhofer, and Kaiming He. Scaling language-image pre-training via masking. In *Proceedings of the IEEE/CVF Conference on Computer Vision and Pattern Recognition*, pages 23390–23400, 2023. 3
- [27] Tsung-Yi Lin, Michael Maire, Serge Belongie, James Hays, Pietro Perona, Deva Ramanan, Piotr Dollár, and C Lawrence Zitnick. Microsoft coco: Common objects in context. In *Computer Vision—ECCV 2014: 13th European Conference, Zurich, Switzerland, September 6–12, 2014, Proceedings, Part V 13*, pages 740–755. Springer, 2014. 7
- [28] Yuqi Lin, Minghao Chen, Wenxiao Wang, Boxi Wu, Ke Li, Binbin Lin, Haifeng Liu, and Xiaofei He. Clip is also an efficient segmenter: A text-driven approach for weakly supervised semantic segmentation. In *Proceedings of the IEEE/CVF Conference on Computer Vision and Pattern Recognition*, pages 15305–15314, 2023. 1
- [29] Ran Liu, Ellen L Zippi, Hadi Pouransari, Chris Sandino, Jingping Nie, Hanlin Goh, Erdrin Azemi, and Ali Moin. Frequency-aware masked autoencoders for multimodal pre-training on biosignals. *arXiv preprint arXiv:2309.05927*, 2023. 2
- [30] Ilya Loshchilov and Frank Hutter. Decoupled weight decay regularization. *arXiv preprint arXiv:1711.05101*, 2017. 7
- [31] Huaishao Luo, Junwei Bao, Youzheng Wu, Xiaodong He, and Tianrui Li. Segclip: Patch aggregation with learnable centers for open-vocabulary semantic segmentation. In *International Conference on Machine Learning*, pages 23033–23044. PMLR, 2023. 2
- [32] Amin Karimi Monsefi, Payam Karisani, Mengxi Zhou, Stacey Choi, Nathan Doble, Heng Ji, Srinivasan Parthasarathy, and Rajiv Ramnath. Masked logonet: Fast and accurate 3d image analysis for medical domain. *arXiv preprint arXiv:2402.06190*, 2024. 1, 2
- [33] Norman Mu, Alexander Kirillov, David Wagner, and Saining Xie. Slip: Self-supervision meets language-image pre-training. In *European conference on computer vision*, pages 529–544. Springer, 2022. 2, 3, 6, 7
- [34] Pouyan Navard and Alper Yilmaz. A probabilistic-based drift correction module for visual inertial slams. *arXiv preprint arXiv:2404.10140*, 2024. 1
- [35] Aaron van den Oord, Yazhe Li, and Oriol Vinyals. Representation learning with contrastive predictive coding. *arXiv preprint arXiv:1807.03748*, 2018. 1, 2
- [36] Maxime Oquab, Timothée Darcet, Théo Moutakanni, Huy V Vo, Marc Szafraniec, Vasil Khalidov, Pierre Fernandez, Daniel HAZIZA, Francisco Massa, Alaaeldin El-Nouby, et al. Dinov2: Learning robust visual features without supervision. *Transactions on Machine Learning Research*, 2024. 2
- [37] Shehan Perera, Pouyan Navard, and Alper Yilmaz. Segformer3d: an efficient transformer for 3d medical image segmentation. In *Proceedings of the IEEE/CVF Conference on Computer Vision and Pattern Recognition*, pages 4981–4988, 2024. 1
- [38] Alec Radford, Jong Wook Kim, Chris Hallacy, Aditya Ramesh, Gabriel Goh, Sandhini Agarwal, Girish Sastry, Amanda Askell, Pamela Mishkin, Jack Clark, et al. Learning transferable visual models from natural language supervision. In *International conference on machine learning*, pages 8748–8763. PMLR, 2021. 1, 2, 3, 6
- [39] Qing Su, Anton Netchaev, Hai Li, and Shihao Ji. Flsl: Feature-level self-supervised learning. *Advances in Neural Information Processing Systems*, 36, 2024. 2
- [40] Bart Thomee, David A Shamma, Gerald Friedland, Benjamin Elizalde, Karl Ni, Douglas Poland, Damian Borth, and Li-Jia Li. Yfcc100m: The new data in multimedia research. *Communications of the ACM*, 59(2):64–73, 2016. 6
- [41] Yonglong Tian, Chen Sun, Ben Poole, Dilip Krishnan, Cordelia Schmid, and Phillip Isola. What makes for good views for contrastive learning? *Advances in neural information processing systems*, 33:6827–6839, 2020. 1, 2
- [42] Hugo Touvron, Matthieu Cord, Matthijs Douze, Francisco Massa, Alexandre Sablayrolles, and Hervé Jégou. Training data-efficient image transformers & distillation through attention. In *International conference on machine learning*, pages 10347–10357. PMLR, 2021. 6
- [43] Zhaoqing Wang, Yu Lu, Qiang Li, Xunqiang Tao, Yandong Guo, Mingming Gong, and Tongliang Liu. Cris: Clip-driven referring image segmentation. In *Proceedings of the IEEE/CVF conference on computer vision and pattern recognition*, pages 11686–11695, 2022. 1
- [44] Yixuan Wei, Yue Cao, Zheng Zhang, Houwen Peng, Zhuiliang Yao, Zhenda Xie, Han Hu, and Baining Guo. iclip: Bridging image classification and contrastive language-image pre-training for visual recognition. In *Proceedings of the IEEE/CVF Conference on Computer Vision and Pattern Recognition*, pages 2776–2786, 2023. 1, 3
- [45] Tete Xiao, Yingcheng Liu, Bolei Zhou, Yuning Jiang, and Jian Sun. Unified perceptual parsing for scene understanding. In *Proceedings of the European conference on computer vision (ECCV)*, pages 418–434, 2018. 7
- [46] Jiahao Xie, Wei Li, Xiaohang Zhan, Ziwei Liu, Yew-Soon Ong, and Chen Change Loy. Masked frequency modeling

- for self-supervised visual pre-training. In *The Eleventh International Conference on Learning Representations*, 2023. [2](#)
- [47] Zhenda Xie, Zheng Zhang, Yue Cao, Yutong Lin, Jianmin Bao, Zhuliang Yao, Qi Dai, and Han Hu. Simmim: A simple framework for masked image modeling. In *Proceedings of the IEEE/CVF Conference on Computer Vision and Pattern Recognition*, pages 9653–9663, 2022. [1](#), [2](#)
- [48] Yifan Yang, Weiquan Huang, Yixuan Wei, Houwen Peng, Xinyang Jiang, Huiqiang Jiang, Fangyun Wei, Yin Wang, Han Hu, Lili Qiu, et al. Attentive mask clip. In *Proceedings of the IEEE/CVF International Conference on Computer Vision*, pages 2771–2781, 2023. [1](#), [2](#), [3](#), [4](#), [5](#), [6](#), [8](#)
- [49] Kun Yi, Yixiao Ge, Xiaotong Li, Shusheng Yang, Dian Li, Jianping Wu, Ying Shan, and Xiaohu Qie. Masked image modeling with denoising contrast. In *The Eleventh International Conference on Learning Representations*, 2023. [2](#)
- [50] Peter Young, Alice Lai, Micah Hodosh, and Julia Hockenmaier. From image descriptions to visual denotations: New similarity metrics for semantic inference over event descriptions. *Transactions of the Association for Computational Linguistics*, 2:67–78, 2014. [7](#)
- [51] Qihang Yu, Ju He, Xueqing Deng, Xiaohui Shen, and Liang-Chieh Chen. Convolutions die hard: Open-vocabulary segmentation with single frozen convolutional clip. *Advances in Neural Information Processing Systems*, 36, 2024. [1](#)
- [52] Behzad Zakeri, Amin Karimi Monsefi, Sanaz Samsam, and Bahareh Karimi Monsefi. Weakly supervised learning technique for solving partial differential equations; case study of 1-d reaction-diffusion equation. In *High-Performance Computing and Big Data Analysis: Second International Congress, TopHPC 2019, Tehran, Iran, April 23–25, 2019, Revised Selected Papers 2*, pages 367–377. Springer, 2019. [2](#)
- [53] Tianyi Zheng, Bo Li, Shuang Wu, Ben Wan, Guodong Mu, Shice Liu, Shouhong Ding, and Jia Wang. Mfae: Masked frequency autoencoders for domain generalization face anti-spoofing. *IEEE Transactions on Information Forensics and Security*, 2024. [2](#)
- [54] Bolei Zhou, Hang Zhao, Xavier Puig, Sanja Fidler, Adela Barriuso, and Antonio Torralba. Scene parsing through ade20k dataset. In *Proceedings of the IEEE conference on computer vision and pattern recognition*, pages 633–641, 2017. [7](#)
- [55] Jinghao Zhou, Li Dong, Zhe Gan, Lijuan Wang, and Furu Wei. Non-contrastive learning meets language-image pre-training. In *Proceedings of the IEEE/CVF Conference on Computer Vision and Pattern Recognition*, pages 11028–11038, 2023. [1](#), [3](#)
- [56] Jinghao Zhou, Chen Wei, Huiyu Wang, Wei Shen, Cihang Xie, Alan Yuille, and Tao Kong. ibot: Image bert pre-training with online tokenizer. *arXiv preprint arXiv:2111.07832*, 2021. [1](#), [2](#), [6](#), [7](#)
- [57] Mengxi Zhou, Yue Zhang, Amin Karimi Monsefi, Stacey S Choi, Nathan Doble, Srinivasan Parthasarathy, and Rajiv Ramnath. Reducing manual labeling requirements and improved retinal ganglion cell identification in 3d ao-oct volumes using semi-supervised learning. *Biomedical Optics Express*, 15(8):4540–4556, 2024. [1](#)
- [58] Ziqin Zhou, Yinjie Lei, Bowen Zhang, Lingqiao Liu, and Yifan Liu. Zegclip: Towards adapting clip for zero-shot semantic segmentation. In *Proceedings of the IEEE/CVF Conference on Computer Vision and Pattern Recognition*, pages 11175–11185, 2023. [1](#), [3](#)

A. Visual Analysis

This section presents a comprehensive comparative analysis of DetailCLIP’s performance against several baseline models, primarily focusing on segmentation and object detection tasks. Through a series of detailed visualizations, we provide side-by-side comparisons that emphasize the superior capability of DetailCLIP in capturing and reconstructing fine-grained details, which is crucial for achieving high segmentation accuracy. Specifically, Figure 4 showcases the semantic segmentation results using the UPerNet decoder, while Figure 5 highlights the results with a linear decoder. These figures emphasize the notable improvements achieved by DetailCLIP in handling complex images, particularly when it comes to accurately delineating boundaries and preserving detailed features, areas where baseline models often struggle. The segmentation comparisons are conducted using the ADE20K dataset.

In addition to segmentation, Figures 6 and 7 present the object detection results using the MS COCO dataset, further demonstrating the effectiveness of DetailCLIP across multiple vision tasks. By visualizing these outputs, we showcase DetailCLIP’s enhanced performance and shed light on the limitations of other models, such as SLIP and A-CLIP. These comparisons underscore the significant advancements made by DetailCLIP in tackling detail-oriented tasks, solidifying its robustness and versatility in a wide array of visual challenges.

Overall, these visual and quantitative evaluations illustrate the significant advancements made by DetailCLIP in addressing detail-oriented challenges across both segmentation and object detection. The side-by-side comparisons solidify DetailCLIP’s robustness and adaptability, making it a more effective and versatile solution for a wide range of fine-grained vision tasks.

Image	Ground Truth	A-Clip	SLIP	DetailCLIP-25	DetailCLIP-50

Figure 4. Visual comparison of segmentation results using the UPerNet decoder across different models. The comparison includes SLIP, A-CLIP, DetailCLIP at 25 epochs, and DetailCLIP at 50 epochs.











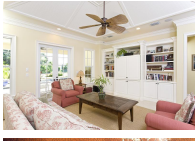










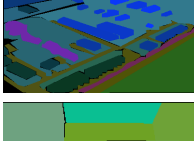
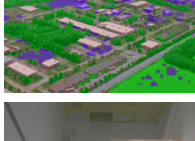



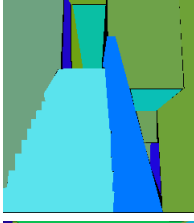
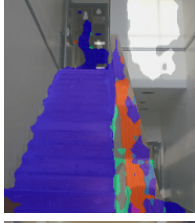
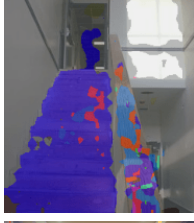
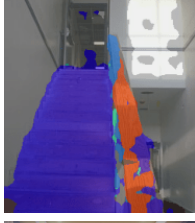
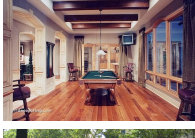












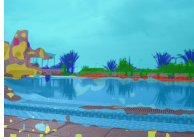

Image	Ground Truth	A-Clip	SLIP	DetailCLIP
				
				
				
				
				
				
				
				
				

Figure 5. Visual comparison of segmentation results using the Linear decoder across different models. The comparison includes SLIP, A-CLIP, and DetailCLIP at 25 epochs.

Image + Objects

Image + Objects



Figure 6. Object detection results using DetailCLIP after 50 training epochs. The image highlights DetailCLIP's ability to detect objects accurately, showcasing its precision and effectiveness in complex scenes

